Solitons Transport Water through Narrow Carbon Nanotubes

Thomas B. Sisan[†]
Department of Physics and Astronomy, Northwestern University, Evanston, Illinois 60208, USA

Seth Lichter[*]
Department of Mechanical Engineering, Northwestern University, Evanston, Illinois 60208, USA

(Received 8 March 2013; published 27 January 2014)

Transformative technologies for desalination and chemical separations call for understanding molecular transport through man-made and biological nanochannels. Using numerical simulation of single-file flow of water through carbon nanotubes, we find that flow is due to fast-moving density variations (solitons) that are additive so flow rate is proportional to number of solitons. Simulation results match predictions from a theoretical model for soliton propagation. From 1–300 K flow rates increase as temperature decreases. Our results build a fundamentally new understanding of nanochannel flows and suggest new principles for the design of nanoscale devices.

DOI: 10.1103/PhysRevLett.112.044501 PACS numbers: 47.61.-k, 05.45.Yv, 47.60.-i

Nanochannels so narrow that flow is restricted to only a single file of molecules, promise transformative technologies such as low-cost desalination and efficient molecular separation and purification [1–3]. Single-file membrane channels such as aquaporin help maintain cellular homeostasis [4]. Despite their biological importance and technological promise, single-file flows are poorly understood. Classical fluid mechanics indicates that intimate contact between water and the channel walls should prohibit flow [5]. Yet, even in onerously restricted diameters, water achieves remarkably high flow rates [6,7]. The prevalent view of single-file flow is that water molecules are evenly spaced and move concurrently [8,9]. This view was supported by prior molecular dynamics (MD) data of water in carbon nanotubes (CNTs) obtained at standard atmospheric conditions (STP). At STP, water molecules on average occupied (6,6) CNTs with approximately 0.93 waters per hexagonal ring [8,10,11], and occupied (5,5) CNTs with approximately 0.86 waters per ring [3,11,12]. Here, by using a wider range of conditions and picosecond resolution, simulations show that the observed average water density is accommodated not by uniform spacing, but by intervals of water molecule registry with carbon rings interspersed with localized regions of mismatch, or solitons. At STP, the solitons are regions of reduced water density. At higher compression, solitons are regions of increased water density. Furthermore, in contrast to expectations that single-file liquids move concurrently, we show that flow of water in CNTs occurs via fast-moving solitons. Predictions from a nonlinear dynamical model of soliton propagation match simulation results [13–19].

We performed a series of MD simulations of TIP3P water in long single-walled (4,4), (5,5), or (6,6) armchair CNTs with periodic boundary conditions [11]. Simulations were composed of isolated CNTs filled with fixed numbers of water molecules. Armchair-type CNT structure is a cylindrical periodic lattice of carbon atoms arranged in hexagon rings with two minima of the potential energy landscape per ring [Fig. 1(a)]. A key simulation parameter was $S \equiv N - L$, the number N of water molecules in surplus over the number L of carbon rings along the axis [15,19]. Simulations conducted at higher (lower) S indicate a relatively greater (lesser) compression of the single file of water molecules. Simulations were conducted over a wide range of S and over a wide range of temperature. Over 5000 simulations were run for a total simulation time of over 40 μs [11].

When the number of water molecules in the CNTs exactly matched the number of rings ($S = 0$), we observed water molecules at every other potential minima, in one-to-one registry with CNT rings, yielding constant density ($\rho_i = 1$) along the length of the CNT [Fig. 1(b)].

When the number of water molecules was one less than the number of rings ($S = -1$), the water molecules could no longer rest evenly spaced in the potential minima. Rather, density always distributed unevenly: most water molecules were spaced in one-to-one registry with the CNT rings, but two localized low-density regions or expansion defects appeared, within which water molecules were more widely spaced [Fig. 1(d)]. Two defects were always found, each defect compensating for half the space of the missing water. Thus, across the width of a defect, the one-to-one registry of the water positions is shifted by one-half of a hexagonal ring [Fig. 1(e)]. For (4,4) CNTs, the width of the defect regions were approximately 1.5 nm; for (6,6) CNTs, approximately 15 nm. A single larger defect, compensating for the whole water molecule, was never observed, and is energetically excluded.

In simulations where the number of water molecules was one greater than the number of carbon rings ($S = +1$), the density increase localized into two high density regions or compression defects where water molecules were spaced more closely than outside of the defects [Figs. 1(h) and 1(i)].

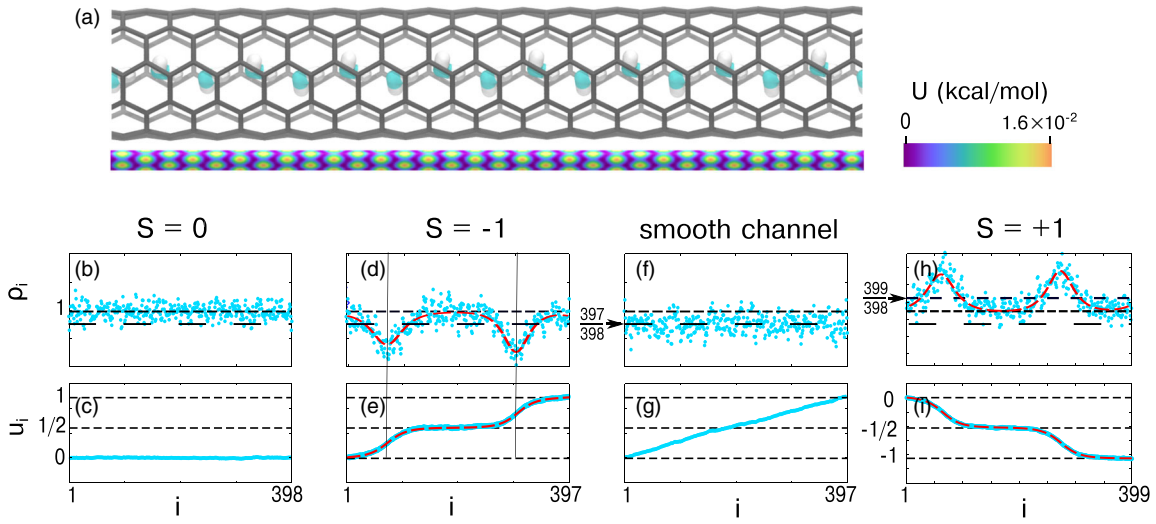

FIG. 1 (color online). Defects in water density are formed when $S \neq 0$. (a) Single-file water (oxygen, blue; hydrogen, white) in a (5,5) CNT with $L = 398$ carbon rings. A 39.3 Å length is shown. The CNT potential energy U evaluated at the mean radial position of the water molecules shows two potential maxima (orange) and two minima (purple) for each carbon ring along the axial direction. (b)–(i) Each blue data point corresponds to a water molecule $i = 1, \ldots, N$. Positions of waters u_i are measured relative to potential minima shown in (a). (b) When $S = 0$, water molecules are spaced one per carbon ring along the length of the CNT so particle density ρ_i is constant for all $i = 1, \ldots, N$ water molecules, and (c) all waters rest in minima of the CNT potential, $u_i = 0$. (d) With one less water ($S = -1$), the reduced density is localized in two defects (centered on horizontal lines). Outside of the defects, the density tends to the same value as for $S = 0$ shown in (b). The MD data are fit by the sech solution (red dashed line) from theory [11]. (e) From the left side of a defect to the right, u_i increases by one-half of the length of a carbon ring as waters are displaced into neighboring potential minima. The MD data are fit by the atan solution (red dashed line) from theory [11]. (f) With one less water, but for an artificially smoothed channel, density is uniform with particles positioned evenly along the channel (g), and no defects are created. (h),(i) Compressive defects ($S = +1$). (b)–(i) Simulations performed at 1 K. At higher temperatures, thermally excited phonon modes are superposed on the defects obscuring their shape (Supplemental Material, Fig. 6 [11]).

(For details of system energies for the cases $S = -1, 0, 1$, see the Supplemental Material [11].) To further determine whether the mismatch between N and L gives rise to defects, we designed a CNT with a potential energy landscape artifically smoothed along the axial direction [11], so that no mismatch was possible. As expected, no defects were created [Fig. 1(f)] and water molecules were equally spaced [Fig. 1(g)].

We next observed the behavior of water molecules near expansion defects as a constant force f was applied to all water molecules. The positions of individual molecules were tracked in time. Water molecules outside of defects remained relatively stationary. But, within the defects, water molecules had forward velocities [Fig. 2(b)]. As defects passed by, water molecules were advanced a distance of one-half the width of the CNT carbon ring into neighboring downstream potential minima [Fig. 2(a)]. Thus, the upstream propagation of defects leads to downstream fluid flow. An analogous phenomenon occurs in a traffic jam: cars are mostly stationary but intermittently move forward into the gap opened by the advance of the preceding car. As cars shift forward, the gap propagates backward (Fig. 3).

To further support our hypothesis that defect motion causes water flow, we tracked defect trajectories over time [Fig. 2(c)] and compared defect velocity against the water flow rate measured directly. Defect velocity correctly predicted flow rates [Fig. 2(d)]. In contrast to classical fluid mechanics and current theories of nanoflow [9,20], which predict flow rate varying linearly with applied force, the defect velocities, and thus the flow rates, varied nonlinearly and were relatively constant over a range of forces (Fig. 4). At lower forces and at room temperature, defect velocities were affected by thermal fluctuations, sometimes reversing direction [Fig. 2(c)] [21]. At higher forces or lower temperatures, defects moved steadily, producing the maximum flow rate [Fig. 4 (inset)]. The behavior of isolated defects under forcing showed similar features in all CNTs and through a range of temperatures (Supplemental Material, Fig. 3[11]).

To determine the dependence of flow rate on the number of water molecules in the channels, we varied S over the range $S = \pm 1, \pm 2, \ldots, \pm 13$. The number of defects observed always equalled $2|S|$. When defects were sparse ($S \approx 0$), flow rates were proportional to the number of defects (Fig. 5). It is striking that the flow rate increased linearly, independent of whether water molecules were removed ($S < 0$) or added ($S > 0$). When defects were crowded ($|S| \gg 0$), flow rates deviated from linearity. Similar effects were observed in all CNTs and for a range of temperatures (Supplemental Material, Fig. 4 [11]).

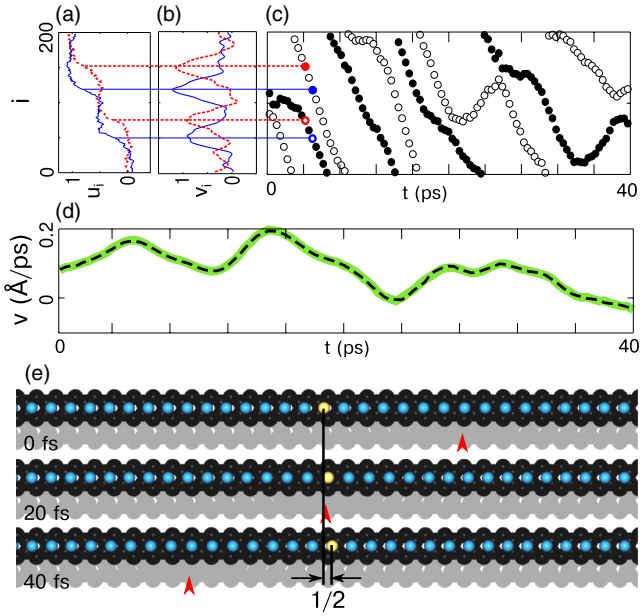

FIG. 2 (color online). Defects convect mass. (a) Displacement u_i of water molecules from their positions at an earlier (red dashed) and 0.8 ps later (blue solid) time. (b) Velocity v_i of water molecules within defects is positive, while outside of defects it is approximately zero, cf. Fig. 3(b). (c) Defect positions as a function of time. The slope of these lines is used to obtain the defect velocities in (d). (d) Water velocity (green line), obtained by averaging the velocity of all waters within the CNT matches well with results from defect tracking (black dashed line). Data from (4,4) CNT with $f = 0.4$ pN at 300 K. (e) For this panel only, the (4,4) diameter was reduced by 5% which reduces the width of a defect so that it and neighboring molecules can be displayed within a reasonably proportioned figure. [Defects in unmodified (4,4) CNTs have the same structure but longer length unsuitable for compact illustration.] Data from a sequence of MD snapshots at three times showing water molecules as (blue and yellow) spheres, carbon atoms as (black) spheres, and the location of the defect (red arrowheads). Top portion of CNT has been removed to reveal water molecule positions; only bottom hexagonal rings remain. Illumination from above. Shadows delineate the location and structure of the defect—light penetrates through the center of the rings, casting bright waxing crescents on the right of the defect; waning crescents are formed on the left. The switch from waxing to waning crescent illustrates the advance (by 1/2 ring length) of waters over the center of the ring. In the region of the defect, the water molecules' positions near the centers of the rings occlude light, casting a full shadow. The defect is seen to span approximately five waters.

Our main findings, that water-CNT incommensuration yields robust density defects that convect mass and are additive, are consistent with features of Frenkel-Kontorova (FK) solitons [21–24]. The FK equations describe the dynamics of particles that interact both with neighboring particles and with a fixed crystalline substrate. The inter-particle interactions alone favor equal spacing of particles at a characteristic length given by the number of molecules and the system size. Particle-substrate interactions alone favor particles resting at the minima of the substrate potential energy. The competition between these two interactions produces solitons, localized variations in particle density [21].

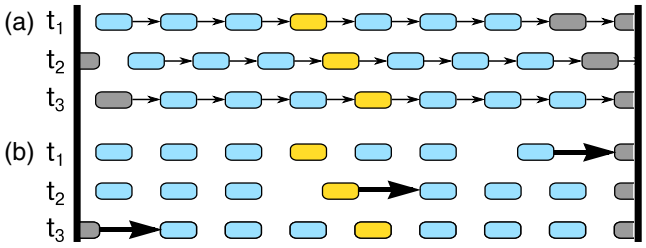

FIG. 3 (color online). Contrasting views of single-file channel transport, shown at three times. (a) In the conventional view, all molecules move as one (aside from thermal motions). (b) Fluid flow by defect propagation. Most molecules are motionless, but near a region of low density, molecules quickly shift positions. The average velocity is the same in (a) and (b). Arrow length is proportional to velocity. Only a short portion of the channel is represented.

In addition to convecting mass, many other observed properties of CNT defects match the characteristics of FK solitons. Here, we summarize these common features (further details are in [11]). (i) Particle displacement and density for FK solitons follow atan and sech distributions, respectively. Water molecules in CNT defects fit well to these distributions [Figs. 1(d), 1(e), 1(h), 1(i), and Supplemental Material, Fig. 6 [11]]. (ii) According to the FK equations, solitons convect mass. Consequently, as the number of solitons decreases, flow rate should decrease to zero. We observed that our measured flow rates approached zero linearly as the number of defects approached zero (Fig. 5 and Supplemental Material, Figs. 4 and 5 [11]). (iii) According to FK theory, on substrates that interact strongly with water molecules, solitons are narrow. CNT defects follow this trend, where defect width decreased as the

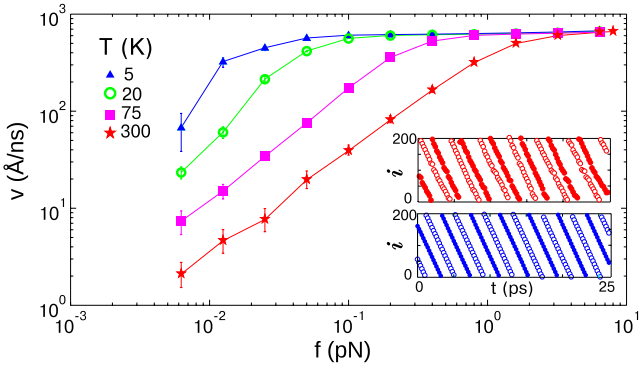

FIG. 4 (color online). At all temperatures T, flow rate v increases with amplitude of external forcing f to a common maximum flow rate. Insets: Defect trajectories as a function of time at high temperature and high forcing, 300 K and 6 pN (red), are similar to those at relatively low temperature and low forcing, 5 K and 0.8 pN (blue). Data from (4,4) CNT with $S = -1$.

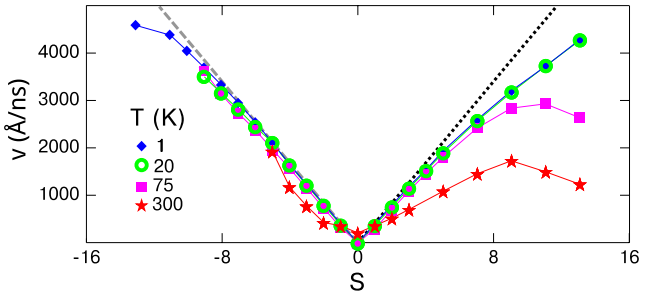

FIG. 5 (color online). Flow rates near $S = 0$ are proportional to the number of defects. When no defects are present ($S = 0$) water molecules reside in potential minima and the flow rate is nearly zero. Flow rates due to expansion defects created by fewer water molecules $S < 0$ lie close to the linear gray dashed line. Flow rates due to compression defects created by additional water molecules $S > 0$ approach the linear black dotted line for small values of S. (5,5) CNT data at $f = 0.02$ pN.

amplitude of the substrate corrugations increased (Supplemental Material, Fig. 7 [11]). (iv) There are two types of FK solitons, kinks and antikinks [21]; when two like solitons approach, they repel one another. We observed that neighboring CNT expansion defects displayed a repulsive interaction (Supplemental Material, Fig. 8 [11]). (v) As the speed of FK solitons increases, their width decreases. In CNTs, when the applied force, and hence the defect speed, increased, the defects also contracted in width (Supplemental Material, Fig. 9 [11]). (vi) As applied force increases, FK solitons approach a maximum speed. Defects showed the predicted asymptotic behavior (Fig. 4 and Supplemental Material, Fig. 3[11]). (vii) When subject to a large force, FK solitons moving at high velocity emit linear waves that carry off energy. CNT defects too, were observed to radiate phonon waves at high applied force (Supplemental Material, Fig. 9 [11]). (viii) As the number of solitons increases, they overlap, and boundaries between solitons can no longer be easily distinguished. A method of plotting solitons when their density is high, called the hull function approach, is borrowed from the FK model and successfully visualizes defects even when they overlap significantly (Supplemental Material, Fig. 2 [11]). At STP defects may overlap significantly [11]. (ix) The FK equations predict that solitons propagate over a wide range of temperatures [21]. In agreement with this result, we observed defect propagation at all temperatures, with thermal fluctuations slowing defects as temperature increased [Figs. 2(c) and 4].

A defect-based mechanism of transport can give new insights and interpretations. Whereas most prior experimental and computational work employed CNTs at standard atmospheric conditions in a narrow range of $S < 0$, our work illustrates defect-based transport by employing a wider range of S. Prior observations of discrete hopping motion of water in short CNTs led to the development of a hopping model based on a continuous time random walk, but gave no mechanism for why unit hops were preferred [25]. Our results present the possibility that transport through long CNTs occurs in discrete units due to soliton propagation. Prior analysis of molecular trajectories suggested concurrent water motion in channels [8]. And, when sampled at traditional MD trajectory time scales on the order of 1 ps, propagation of large-width overlapping solitons gave the appearance of concurrent motion. However, low-temperature finer-grained time sampling on the order of 10 fs revealed pulse propagation at the speed of the soliton. Furthermore, for water molecules to move concurrently, as assumed by other models of CNT flow, applied pressures must be high enough to move the entire single-file length of molecules simultaneously. In contrast, only the subset of molecules within a localized region must be set in motion to initiate soliton propagation. Thus, fast pressure-driven flow occurs at low applied pressures [2,7,26]. Our simulations on infinite CNTs gave flow rates comparable to those found in the biological transmembrane channel aquaporin, after accounting for end effects [20] and after matching aquaporin radii [11].

Our results and analysis introduce a new mechanism of rapid single-file flow in nanochannels which accords with prior observations of discrete, but not concurrent, molecular hopping. Defects are shown to possess many of the characteristics of FK solitons, which argues for competition between two length scales—water-water spacing versus carbon-carbon spacing—as the mechanism underlying defect formation. As this competition is present in all similarly filled nanochannels, such as BNNTs, SiCNTs, and larger CNTs, and for any fluid molecule, it may be worthwhile to investigate if defects play a role in transport in a wider range of nanochannels [27] and for diverse fluids. As this competition is independent of temperature, liquids flow at low temperatures. The FK model is parametrized by the water surplus S, the relative strength of the water-water interaction compared with the water-CNT interaction, and the friction between the water and the CNT. As the FK model agrees well with numerical simulation of water dynamics within a CNT structure, these three parameters provide a basis for exploring transport characteristics of nanochannels. Augmenting the model to more accurately represent local and nonlocal interactions, flexibility, polarization, and high-temperature effects, may provide a comprehensive explanation of the flow of water and other molecules in nanochannels.

Financial support of the Lillian Sidney Foundation is gratefully acknowledged. MD simulations were supported by Northwestern University's QUEST HPC.

*Corresponding author.
s-lichter@northwestern.edu
†tbsisan@northwestern.edu

[1] C. R. Martin and P. Kohli, Nat. Rev. Drug Discovery 2, 29 (2003).

[2] B. J. Hinds, N. Chopra, T. Rantell, R. Andrews, V. Gavalas, and L. G. Bachas, Science **303**, 62 (2004).
[3] B. Corry, J. Phys. Chem. B **112**, 1427 (2008).
[4] B. L. de Groot and H. Grubmüller, Science **294**, 2353 (2001).
[5] G. K. Batchelor, *An Introduction to Fluid Dynamics* (Cambridge University Press, Cambridge, UK 1967).
[6] M. Majumder, N. Chopra, R. Andrews, and B. J. Hinds, Nature (London) **438**, 44 (2005).
[7] J. K. Holt, H. G. Park, Y. Wang, M. Stadermann, A. B. Artyukhin, C. P. Grigoropoulos, A. Noy, and O. Bakajin, Science **312**, 1034 (2006).
[8] G. Hummer, J. C. Rasaiah, and J. P. Noworyta, Nature (London) **414**, 188 (2001).
[9] F. Zhu, E. Tajkhorshid, and K. Schulten, Biophys. J. **86**, 50 (2004).
[10] B. Mukherjee, P. K. Maiti, C. Dasgupta, and A. K. Sood, J. Chem. Phys. **126**, 124704 (2007).
[11] See Supplemental Material at http://link.aps.org/supplemental/10.1103/PhysRevLett.112.044501 for further details of experimental methods and interpretation of results.
[12] A. Alexiadis and S. Kassinos, Chem. Eng. Sci. **63**, 2047 (2008).
[13] J. Koplik, J. R. Banavar, and J. F. Willemsen, Phys. Fluids A **1**, 781 (1989).
[14] P. A. Thompson and M. O. Robbins, Phys. Rev. A **41**, 6830 (1990).
[15] J.-L. Barrat and L. Bocquet, Faraday Discuss. **112**, 119 (1999).
[16] S. Lichter, A. Roxin, and S. Mandre, Phys. Rev. Lett. **93**, 086001 (2004).
[17] S. M. Saparov, J. R. Pfeifer, L. Al-Momani, G. Portella, B. L. de Groot, U. Koert, and P. Pohl, Phys. Rev. Lett. **96**, 148101 (2006).
[18] A. Kalra, S. Garde, and G. Hummer, Eur. Phys. J. Spec. Top. **189**, 147 (2010).
[19] K. Falk, F. Sedlmeier, L. Joly, R. R. Netz, and L. Bocquet, Langmuir **28**, 14261 (2012).
[20] T. B. Sisan and S. Lichter, Microfluid. Nanofluid. **11**, 787 (2011).
[21] O. M. Braun and Y. S. Kivshar, Phys. Rep. **306**, 1 (1998).
[22] S. N. Coppersmith and D. S. Fisher, Phys. Rev. A **38**, 6338 (1988).
[23] D. W. McLaughlin and A. C. Scott, Phys. Rev. A **18**, 1652 (1978).
[24] T. Strunz and F.-J. Elmer, Phys. Rev. E **58**, 1612 (1998).
[25] A. Berezhkovskii and G. Hummer, Phys. Rev. Lett. **89**, 064503 (2002).
[26] M. Majumder, N. Chopra, and B. J. Hinds, ACS Nano **5**, 3867 (2011).
[27] A. Vadakkepatt, Y. Dong, S. Lichter, and A. Martini, Phys. Rev. E **84**, 066311 (2011).